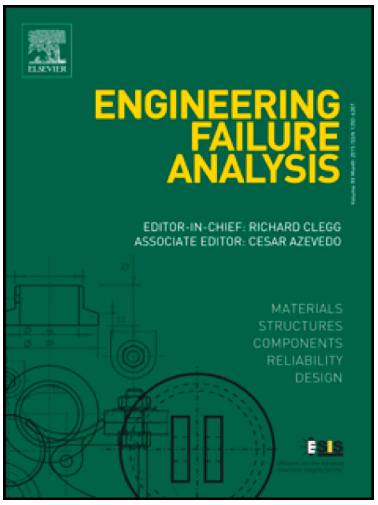

Fracture Surface Analysis and Quantitative Characterization of Gallium Arsenide III-V Semiconductors using Fractography

Anthony Moulins, Roberto Dugnani, Ricardo J Zednik

PII: S1350-6307(21)00101-1
DOI: https://doi.org/10.1016/j.engfailanal.2021.105313
Reference: EFA 105313

To appear in: *Engineering Failure Analysis*

Received Date: 2 September 2020
Revised Date: 9 February 2021
Accepted Date: 9 February 2021

Please cite this article as: Moulins, A., Dugnani, R., Zednik, R.J., Fracture Surface Analysis and Quantitative Characterization of Gallium Arsenide III-V Semiconductors using Fractography, *Engineering Failure Analysis* (2021), doi: https://doi.org/10.1016/j.engfailanal.2021.105313

Fracture Surface Analysis and Quantitative Characterization of Gallium Arsenide III-V Semiconductors using Fractography

Anthony Moulins[1], Roberto Dugnani[2,a] and Ricardo J Zednik[1,b]

[1]École de Technologie Supérieure, Université du Québec, Montréal, Canada
[2]University of Michigan - Shanghai Jiao Tong University Joint Institute, Shanghai, China

ABSTRACT

Gallium arsenide (GaAs) is used in the most demanding semiconductor applications, including the medical, aerospace and communication industries, where significant mechanical stresses are experienced during operation. Mechanical stresses from thermal expansion and mechanical loading can result in the fracture of GaAs crystals, a leading cause of semiconductor device failure. Unfortunately, the underlying fracture mechanisms in GaAs III-V semiconductors are currently not well understood. In this manuscript, we present a quantitative approach to identify the main GaAs fractographic features and correlate these to a crystal's original mechanical fracture strength. In addition, detailed fractographic analysis was used to estimate the crystal hackle constant (analogous to the mirror constant in isotropic media), = 1.58 MPa√m on the {110} cleavage plane of GaAs. Finally, crystal stereography and analytical geometry was used to confirm that the fractographic features correspond to the intrinsic symmetries of single-crystal GaAs.

Keywords: fractography, failure analysis, single crystal, gallium arsenide, mirror constant, crystal hackle, stereography

[a] Corresponding author: roberto.dugnani@sjtu.edu.cn
[b] Corresponding author: ricardo.zednik@etsmtl.ca

Authors' accepted manuscript. Article published in *Engineering Failure Analysis*, Volume 123, May 2021, 105313
The final publication is available at https://doi.org/10.1016/j.engfailanal.2021.105313

I. INTRODUCTION

GaAs exhibits superior semiconducting properties compared to silicon and germanium, including higher charge carrier mobility, a direct band-gap transition, and improved power and high-frequency response[1,2]. GaAs is therefore particularly useful in advanced optoelectronic and photonic devices, as well as in ultra-high frequency and microwave applications. GaAs displays excellent resistance to radiation and thermal degradation, making it valuable for space applications and super-efficient photovoltaic cells[3,4]. However, mechanical stresses during processing and operation can lead to catastrophic brittle fracture of GaAs crystals, a significant cause of semiconductor device failure[5]. Analyzing the fracture surface of a failed device or structure is a standard approach commonly used in failure analysis in order to identify the root cause. Unfortunately, the mechanisms by which single crystals, including GaAs, fracture or crack is poorly understood.

Basic fractographic concepts for single crystals began to be developed in the 1940s[6–11]. Margevicius and Gumbsch[12] studied the behavior of GaAs fractures, and observed that as GaAs cleaved on {100} and {111} planes, the crack eventually deflected onto {110} planes, but provided no explanation. Okui et al.[13] studied GaAs cleavage by scanning tunneling microscopy and revealed that, in contrast with [110] cleavage, cleaving toward [112] and [114] resulted in flat (110) terraces. In addition, many elongated “island-like” structures and high step densities were detected, however, they were “largely fluctuating” in the scans and the authors were not able to correlate them with any particular crystallographic directions. Sauthoff et al.[14] separated the fracture surface of GaAs into six regions of interest, each with characteristic morphologies. Although each morphology was associated with a distinct crack front velocity, the authors did not formerly correlate these findings with the intrinsic anisotropy of the crystal and the loading direction.

When performing the fractographic analysis of isotropic brittle materials, such as glasses or fine-grained ceramics, the distance between the origin and the mirror-mist boundary is

correlated to the strength of the material by a phenomenological expression first formalized by Orr[15] :

(1)

where σ_f is the strength, R_m is the mirror radius, and A_m is the empirically obtained, material-dependent mirror constant[16]. Macroscopically, in glasses and fine ceramics, the onset of crack growth instabilities delineates the mirror-mist boundary or the mist-hackle boundary regions[17–19]. For single crystals, the crack-front first propagates on a characteristic mirror-like plane i.e. weakest cleavage plane, but once the crack-tip reaches a critical, characteristic speed along a specific crystallographic direction, micro-branching occurs[10,20–23]. In the past, various authors attempted to apply variations of Orr's equation to single crystals but did not formally provide any "standardized" methodology on how and where to measure the mirror radius[10,15,24–27]. Not surprisingly, A_m was found to depend on the crystalline plane considered, the loading direction, and the observation technique used, such as, for instance, in single-crystal silicon[28]. Nonetheless, no study has been conducted to formally establish a relationship between fractographic features and the strength of GaAs prior to this work.

In this manuscript, we therefore develop a fractographic approach to establish the mechanical fracture strength of GaAs based on characteristic fractographic features. In order to remain consistent with the literature, we use the same definition of fracture strength used by Orr[15]. This fracture strength is the stress required for a crack to propagate catastrophically through a crystal; as fracture initiates at natural flaws that are present in any crystal, we would expect a Weibull-type relationship between strength and specimen size; in order to eliminate this effect, all tested samples had the same geometry and dimension.

The manuscript begins by describing the experimental set-up used to fracture GaAs single crystals before proceeding to discuss, in detail, the fracture surfaces obtained. The fractographic features discussed are important in order to generalize Orr's relation for isotropic media to single crystal GaAs. This work accounts for the crystal orientation and uses fractographic analysis to determine the crystal hackle constant, on the {110}

cleavage plane and measured along the directions, analogous to the mirror constant in isotropic media.

II. METHODOLOGY

This section provides details on the characterization techniques and proposes a quantitative fractographic approach to establish the relationship between the fracture surface's fractographic features and the crystal strength of GaAs.

A. Uniaxial Flexural Tests

Undoped GaAs wafers (nominal 3-inch diameter) with one side mirror-polished and a thickness h = 619 ± 19 μm were cleaved along the (110) plane. Uniaxial flexural overloading was performed on 25 specimens by three-point bending tests (3PBTs) according to the ASTM C1161 standard[29] as presented in Figure 1. The test specimens corresponded to the ASTM C1161 size and geometry requirements, and were rectangular bars with widths b = 8 ± 2 mm and useful test length l = 41 ± 10 mm. The 3PBTs were conducted on an MTS system with a 50N load cell (resolution 0.01 N) and roller diameter 10 mm. Test specimens were loaded using displacement control at a fixed speed of 0.5 mm/min. The cracks were initiated at natural flaws on the mirror-polished side to avoid any strong flaw misorientation. The fracture strength σ_f reported throughout the manuscript corresponds to the experimentally measured stress imposed by the 3PBT at which fracture occurred. Small deflection and linear elastic response during experiments justify the use of linear elastic beam theory to calculate the stress at failure. According to ASTM C1161, the flexural stress at failure is therefore given by

, (2)

where P is the fracture force.

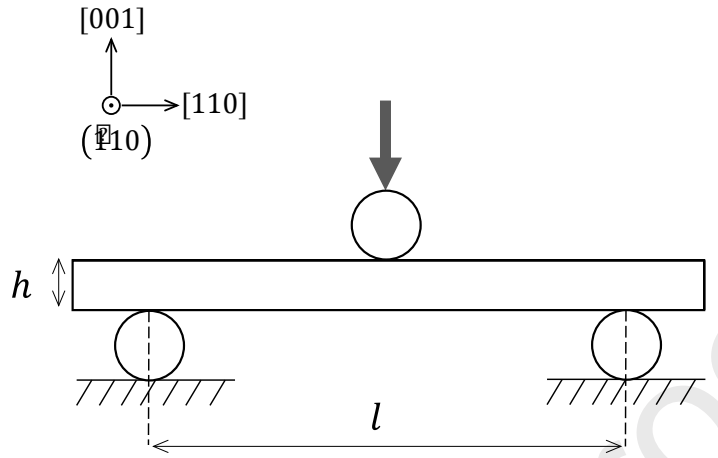

Figure 1: Schematic of the experimental three-point bending test (3PBT) setup showing GaAs crystal [110] orientation. The polished surface is on the bottom (tension) side.

B. 3D Surface Characterization

An Olympus LEXT OLS4100 confocal microscope was used to identify fractographic characteristics with the help of Matlab[30] to extract and analyze post-mortem fracture surfaces. Fracture surface 2D micrographs and 3D maps were obtained with bright field illumination and through a non-polarized, 405 nm ultraviolet laser source, resulting in a nominal 10 nm height resolution and 120 nm lateral resolution.

C. Crack Growth Analysis

As GaAs fractures in an anisotropic manner, the crystal's hackle radius could be influenced by any misalignment of the load with respect to [110]. In order to identify such misalignment, the sample orientation must be carefully established to ensure perpendicularity of the mirror plane with the optical/confocal microscope axis. The following standardized algorithm was used as the basis of a concise standardized failure analysis procedure when characterizing single-crystal GaAs fracture surfaces:

(1) Confocal optical micrographs near the fracture origin are collected with each fracture surface oriented with the free surface parallel to ¯. As the mirror region near the origin is generally not perfectly aligned with the optical axis, i.e. aligned with [110], the region near the origin is leveled by fitting a plane to the flat mirror region and rotating the mirror to align with [110].

(2) The location of the crack's origin locus is visually confirmed by back-tracing the source of the "quasi-static" step-like features, as described in the next section.

(3) The radii at branching are measured optically using semi-circular arcs centered at the crack's origin and tangent to the first occurring branching ridges. Underestimation of the hackle radius could be introduced due to limitations in the resolution of the measuring equipment. Fractographers need to ensure that the incident radiation wavelength is sufficient to detect features with adequate resolution and should be capable of interpreting relevant fractographic markings. In this work, the crack-tip paths were tracked with 10 nm height resolution and 120 nm lateral resolution. Methodology to confirm the hackle radius based on the height of the steps or ridges is explained in later sections.

(4) The distance between the crack origin and first crack-branching steps or ridges are used to define the crystal hackle (or mirror) radii. For specimens that broke both 'at the edge' and 'away from the edge', $R_{XH\{110\}}$ was measured along ¯.

(5) The crystal hackle constant is obtained correlating the strength with the reciprocal square root of the crystal hackle radii on (110) towards ¯.

(6) The hackle directions, φ_i, are estimated optically on the sample with respect to ¯ at the free surface, as shown in Fig. 6 (a). The local crack-tip branching deflection angles, θ_B, with respect to the (110) mirror plane normal vector can be computed from laser profilometry (LP) with a 3D UV-laser confocal microscope, as shown Figs. 7-8. The theoretical values for φ_i and θ_B can be

computed using trigonometry from the planes for any desired crystal. Crystal stereography can then be used to help confirm that the indexed planes and axes were satisfy the intrinsic crystal symmetries of GaAs.

III. RESULTS

A. Misalignment of Mechanical Load

All of the GaAs specimens initially fractured on {110} planes by a cleavage-step mechanism systematically forming a “flat” mirror region. ‘Step-like’ features fracturing along the (110) planes were observed fanning directly from the fracture origin as, for instance, shown in Figure 2.

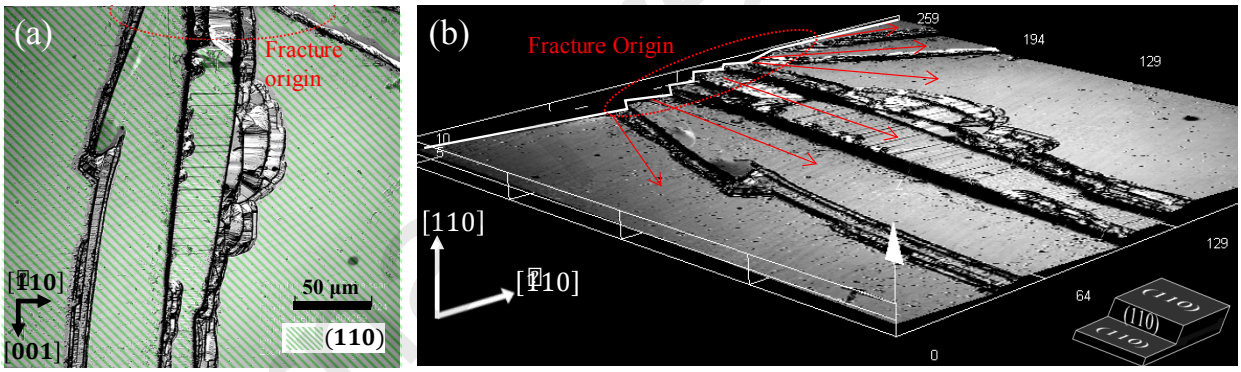

Figure 2: (a) 2D Confocal micrograph of a representative (110) GaAs stepped fracture surface and (b) 3D micrograph of same fracture surface showing misalignment between the main cleavage plane (110) and the fracture origin

For the case shown in Figure 2, the stepped fracture surface was introduced by the misalignment between the main cleavage plane (110) and the crack origin, which essentially provided multiple crack initiation seeds for the crack to propagate on parallel {110} planes.

Another instance of GaAs's step-deflection mechanism on a different sample is shown in Figure 3, where cracks propagate with a small misalignment, α_1, with respect to the loading direction.

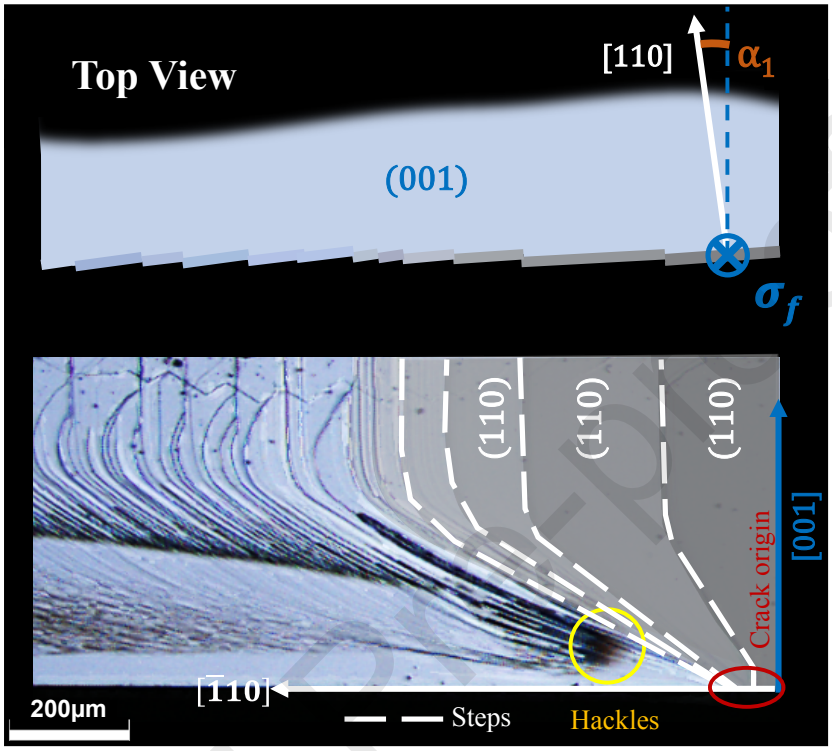

Figure 3: Terrace-like steps (or ridges) due to small misalignment between the loading direction and the cleavage plane.

These features remained on the plane of the crack and did not seem to contribute significantly to the macroscopic change in the crack propagation direction. Terrace-like steps fan directly from the fracture origin to compensate for the α_1 misalignment between [110] and the loading direction [001].

B. Hackle Branching

In order to enable a quantitative analysis of fracture surfaces, the "hackle branching" feature was identified as an important fractographic feature. This allows us to define a "crystal hackle radius" R_{XH} (for a given crystallographic direction) in single crystal GaAs that is analogous to the "mirror radius" R_m normally used to study the fracture of isotropic materials. Additional hackle features out of the (110) mirror plane were found fanning

away from the crack origin delineating “wing-like” branching regions. Figure 4(a) and 4(b) show instances of fractures with the origin “away from the edge” and with the fracture origin “at the edge”; as expected, no significant fractographic differences were noted between the two cases. Figure 4(a) and 4(b) show representative fracture surfaces where a high-density of hackle lines are present away from the crack origin. Steps are running toward the upper right (compressive) side of the specimen from the crack origin, almost perpendicular to the propagating crack-front (dashed line).

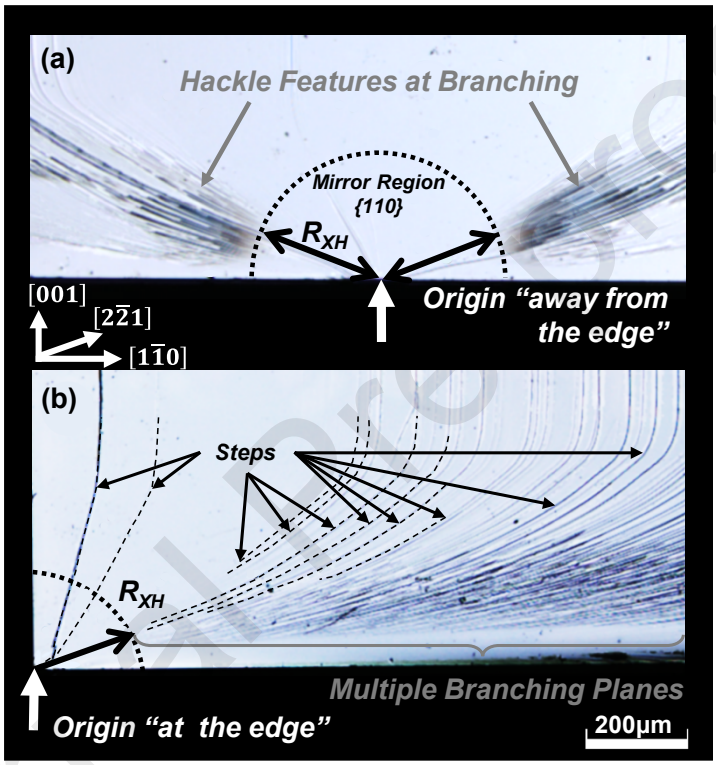

Figure 4: (a) Representative fracture surfaces of GaAs with origin away from the edge (σ_f=95±5MPa), and (b) at the edge (σ_f=148±8MPa).

The flat fracture surface in Figure 4 was associated with the principal (110) cleavage plane surrounding the crack origin and is known as the mirror region. The fracture strength σ_f corresponds to the experimentally measured stress at fracture. Various (110) ‘step-like features’ were observed fanning out from the fracture origin and were associated the maximum tensile stress not being perfectly aligned with the (110) cleavage plane.

For the fracture surfaces observed across all samples, two distinct sets of hackle lines with the same fractographic pattern were systematically produced. In Figure 5, the 3D surface profilometry of a representative specimen obtained near the beginning of hackles (i.e. the onset of branching at the mirror-hackle boundary) is shown. Figure 5 shows how the crack branches away from the (110) mirror plane with hackles oriented mostly towards ¯. For the sample shown in the Figure 5, $R_{XH\{110\}}$ ~151 μm and σ_f = 83 ± 6 MPa. Shorter hackles (delimited by the dashed line) alternate with the larger hackles. The beginning of the crack branching was characterized by sharp hackles visible at the microscale, thus delineating a transition between a nearly flat mirror region and the hackle features.

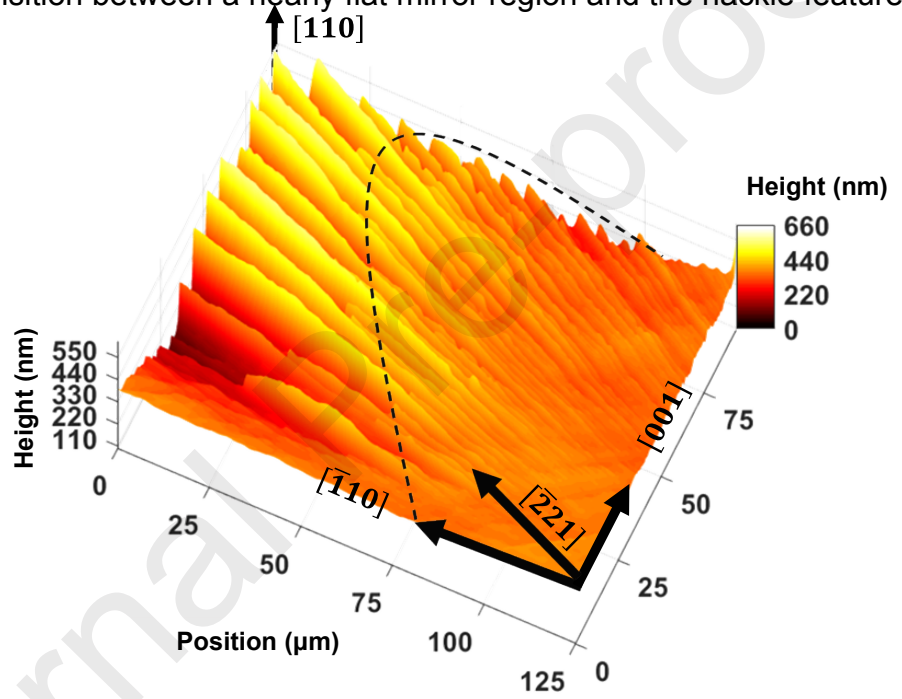

Figure 5: Representative fracture surface of GaAs at branching (σ_f=83±6MPa).

The hackle directions with respect to ¯ at the free surface, , were estimated optically on the sample as shown in Fig. 6 (a).

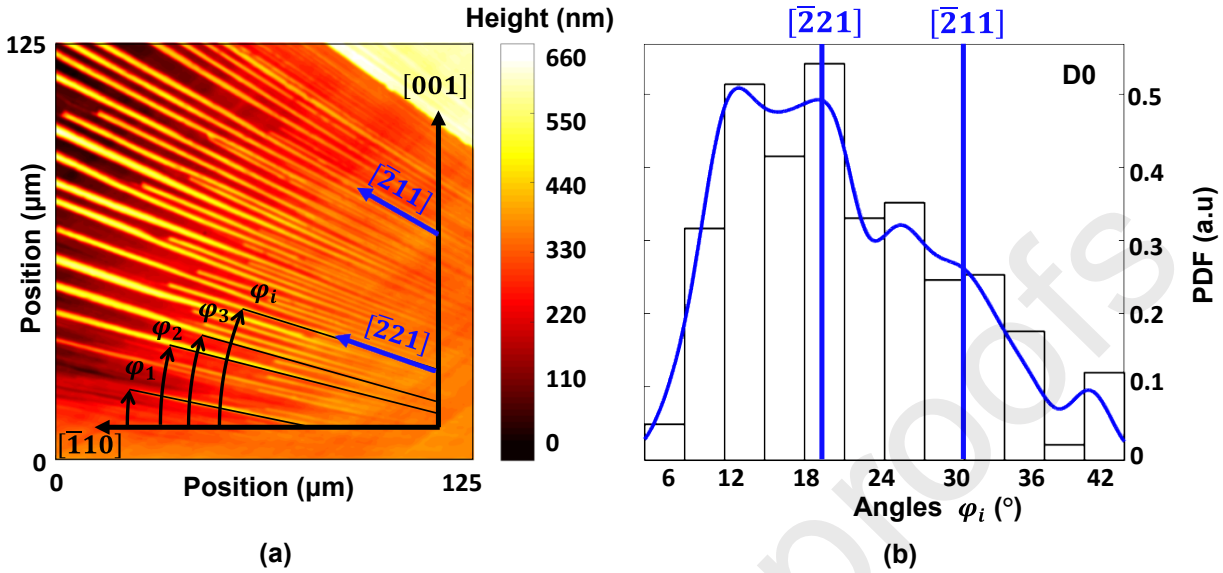

Figure 6: (a) Representative micrograph of GaAs fracture surface near the onset of crack branching and (b) probability density function (PDF) of the GaAs feature's directions with respect to ¯ (same sample as shown in Figure 5)

Fig. 6(b), shows an example of the Kernel density estimator (KDE) for the hackle directions (blue envelope). The KDE is a smoothing function that establishes the shape of the curve based on the probability density function (PDF). The bin sizes (column widths) were selected from Scott's rule i.e. asymptotically minimizing the integrated mean squared error. The distribution of hackles within branching is mostly attributed to ¯, although hackles were found within $\varphi_{min} = 6° < \varphi_i < 42° = \varphi_{max}$.

For hackles oriented within the interval φ_{min} and φ_{max}, the crack-front shape remains perpendicular to the branching features (i.e. nearly circular with respect to the crack origin), as shown in Figure 7. Profile P1 was obtained at radius R1 ≈ $2R_{XH\{110\}}$ (i.e. ~ 302 μm) from the crack origin. The height (i.e. the hackle's height or amplitude) was approximately $\delta_1 \approx 472$ nm and the "contour" triangular and elongated. For profile P2 (at R2 ≈ $1.7R_{XH\{110\}}$), the hackle height was approximately $\delta_2 \approx 280$ nm and for profile P3 (at R3 ≈ $1.4R_{XH\{110\}}$), the hackle height was approximately $\delta_3 \approx 138$ nm.

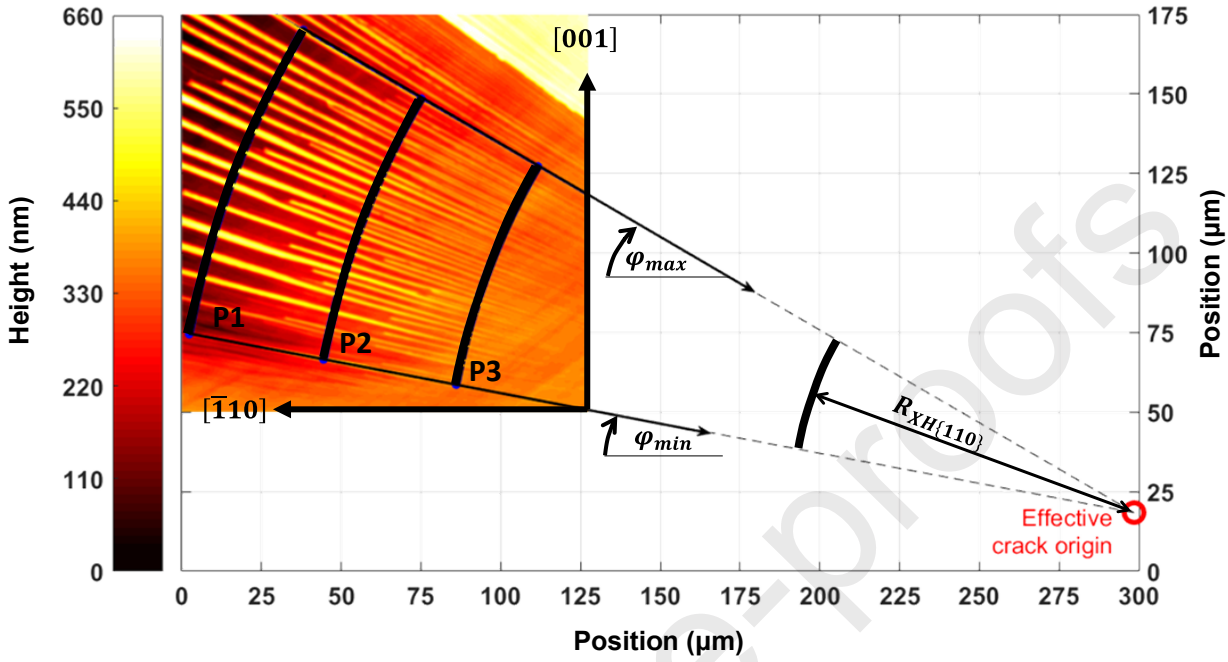

Figure 7: Identification of the crack front profiles P1 ≈ 2$R_{XH\{110\}}$, P2 ≈ 1.7$R_{XH\{110\}}$ and P3 ≈ 1.4$R_{XH\{110\}}$ for $R_{XH\{110\}}$=151μm and the effective crack origin locus (same sample as shown in Figures 5 and 6).

The hackle heights (Pi) from P1, P2 and P3 have been normalized by radial distances R1, R2 and R3, respectively to obtain Figure 8 (a). Figure 8 (b) shows the distributions D1, D2 and D3 of the angles obtained from P1, P2 and P3. The hackles' orientations were computed directly from 3D LP with respect to . Figure 8 (a) shows that the density of peaks from P1 to P3 decreases as the distance between the crack-origin and the crack-front increases, and the most prominent hackles at P1 appear to correspond to the {111} planes and {454} planes which are very close to each other ~2.7º. Large branching features with low density were apparent (P1) as the crack propagated farther from the crack origin, whereas small and narrowed branching features with higher density were present (P3) in the early crack branching process.

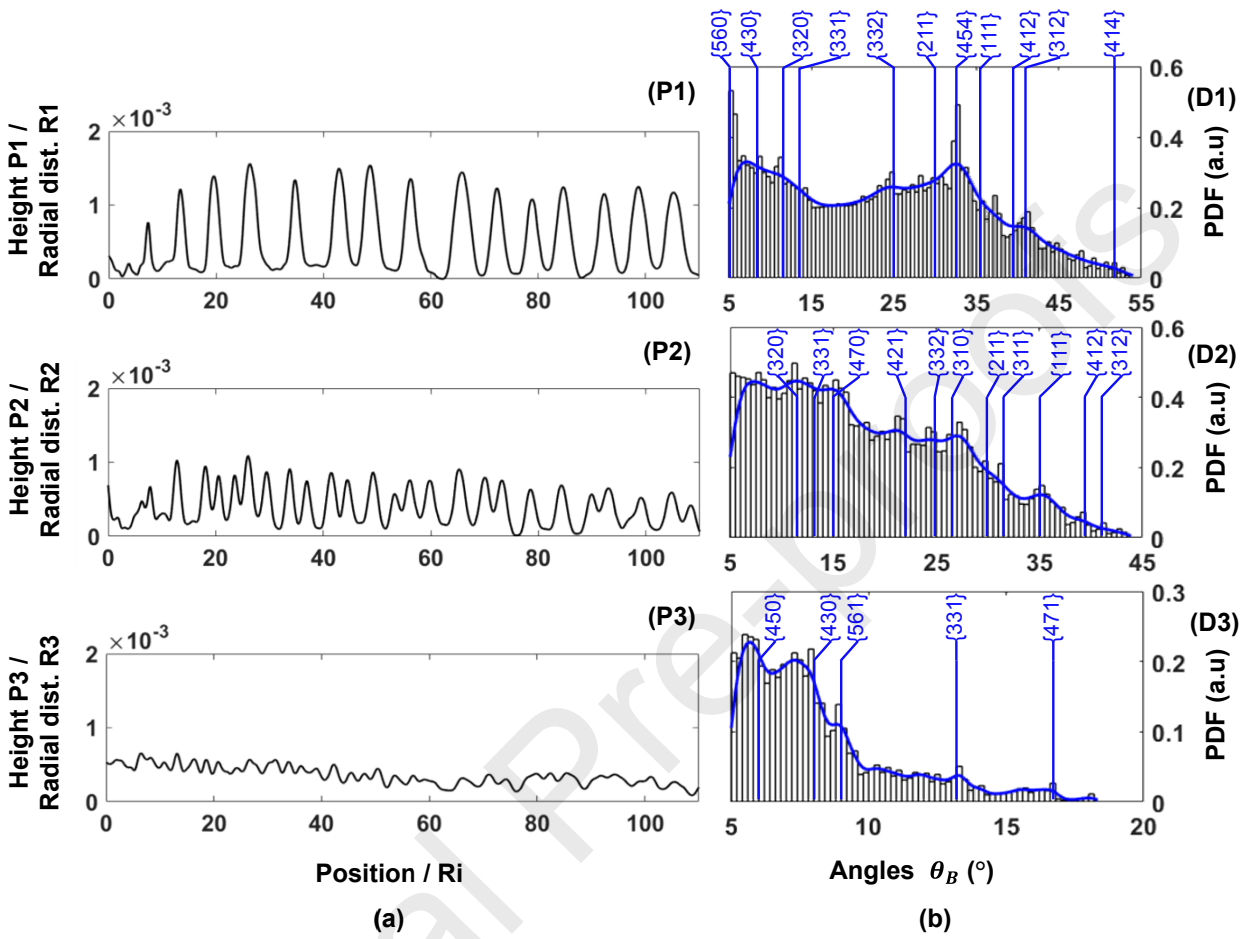

Figure 8: (a) Normalized height profilometry (P1, P2 and P3) with radial crack-lengths R1, R2, R3 and (b) resulting distributions (D1, D2 and D3) of GaAs surface angles

The profile P1 shows a periodicity in the ridges with an average lateral distance between peaks of $\overline{K}$ 1644 nm with an angle between peaks of ζ_1 ~ 0.31° with respect to the crack's origin. This angle was calculated using the law of cosines (Al-Kashi theorem):

$$\overline{K} \qquad (3)$$

The distribution D1 shows that the range of the facet orientations is between 5-55°. P2 shows a slightly less recurring surface profile in Fig. 8 (b). The distribution D2 shows that

the range of the facets orientations is between 5-45°. The average lateral distance between each peak in P2 is $\bar{K}$ 936 nm with an angle between peaks of ζ_2 ~ 0.21º. Furthermore, LP highlighted a tortuous crack path at the onset of the crack branching in the region of P3 where locally, a high density of ridges (i.e. hackle features) were present. However, P3 does not seem to follow any regular cracking sequence and most probably the feature size could not be easily detected because of the optical limitations imposed by the incident radiation wavelength (i.e. 405nm). The corresponding distribution D3 shows that the range of the facets' orientations is between 5-19°. Although local maxima of D3 are relatively close to each other, D3 indicates that there are traces of the crack-tip deflecting out of (110) with a relatively high density of the Kernel estimator. The average lateral distance between each peak in P3 is $\bar{K}$ 677 nm with an angle between peaks of ζ_3 ~ 0.18º.

C. Deflection Planes Correlate with the Crack's Zone Axis

Stereographic projections of GaAs were used to identify the crystal directions of fractographic features observed on all samples. For this analysis, the relevant cracking sequence along P1 corresponding to angular surface distribution D1 was selected. D1 therefore corresponds to the angular surface distribution relative to the mirror direction and D0 corresponds to the angular surface distribution relative to the free edge direction ¯. Figure 9 (a) shows the crystallographic directions of experimentally observed crack deflection planes at branching that lie within 5-55° from (110), such as {331}, {231}, {221}, {241}, {130}, {131}, {121}, {111}, {142}, {132}. Great circles corresponding to these crystallographic directions are shown in Fig. 9 (b)-(c)-(d)-(e). The intersection of each of these great circle traces with the main (110) trace provides the effective crystallographic direction indices (i.e. effective zone axis) of the crystal hackle radius at branching.

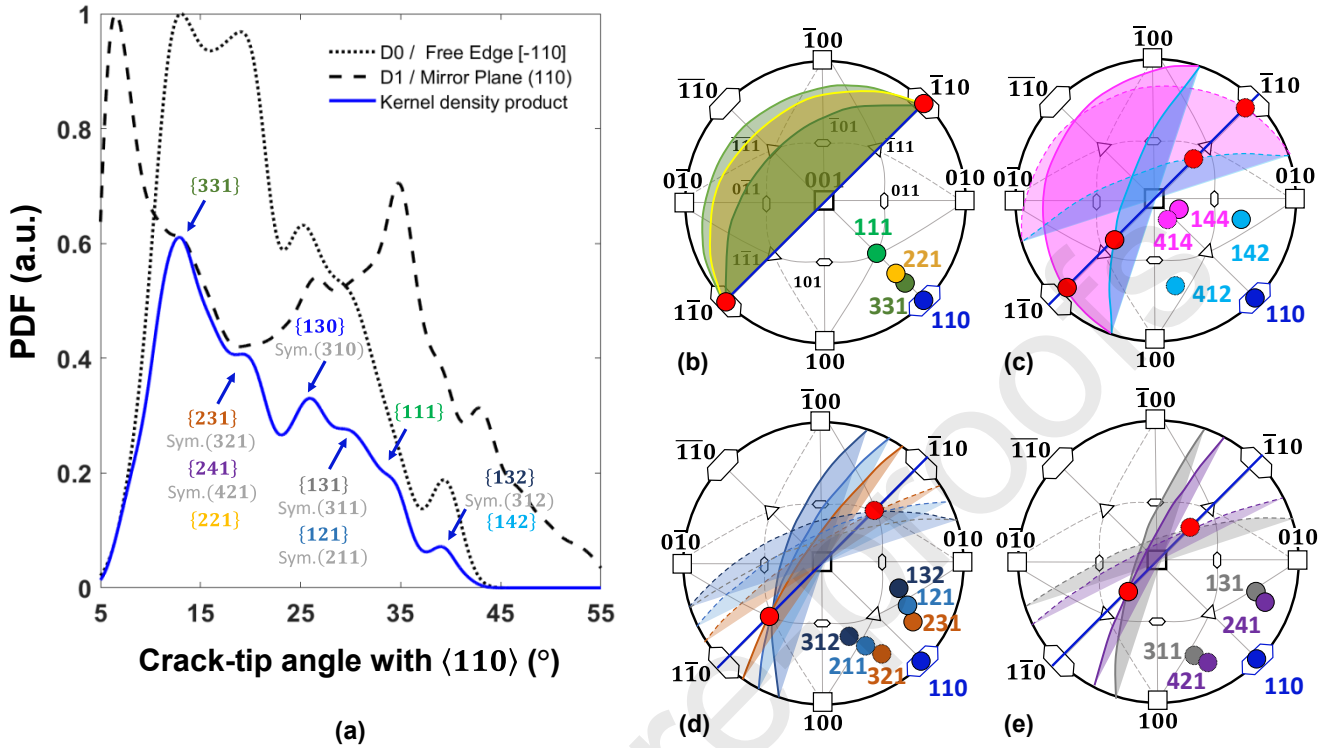

Figure 9: (a) Experimentally observed Probability Density Function (PDF) of crack-tip branching angles relative to (110) as observed in all tested samples, and (b)-(c)-(d)-(e) stereographic projections with directions and traces of the fracture planes in GaAs single crystal

In order for the experimentally observed deflection planes at branching to be consistent with GaAs crystal symmetry and the experimental hackle radius directions, the Weiss zone law (WZL) must be satisfied[31–33]. As shown in Figure 9, we indeed confirm that the deflection planes which were in the zone axis followed WZL, and by extension were also in the same family of planes containing the indices of the effective crystallographic directions of $R_{XH\{110\}}$. The crack cleavage planes were formed from five groups of zone axes (i.e. hackle directions):as shown in Figure 9 (b)-(c)-(d)-(e), the red dots represent the intersection of the trace of (110) (straight blue line) with the traces of the deflecting planes (solid-colored arcs). The dashed arcs represent the great circles and each intersecting point indices can be obtained by superimposing a full (001) stereogram[31]. For

example, Figure 9 (b) shows that the {111}, {221}, and {331} traces intersect the (110) trace at ¯ and the ¯ trace at ¯. This confirms that {111}, {221} and {331} intersect {110} at a direction parallel to the free surface and rotate toward the [001] to align with the macroscopic principal stress. Figure 9 (c) shows that {144} and {142} intersect (110) at ¯ and ¯, respectively, consistent with the crystal symmetry. Figure 9 (d) shows that {132}, {121} and {231} intersect (110) at ¯ and ¯, respectively. Figure 9 (e) shows that {131} and {241} intersect (110) at ¯ and ¯¯, respectively. In summary, the experimental observations are consistent with the crystal symmetry of GaAs.

D. Hackle Radius versus Mechanical Strength

Figure 10 shows the stress at failure σ_f as a function of the crystal hackle radius; this stress corresponds to the experimental stress imposed by the 3PBT at the point of failure. The value of the stress was determined from the mechanical load imposed by the 3PBT set-up at the time of catastrophic fracture as calculated according to the ASTM C1161 standard[29].The uncertainties were estimated using a statistical propagation of uncertainty approach using the variance of individual measurements. As shown in Fig. 4, mirror radii were estimated optically and were mostly oriented towards ¯ (~19.5° away from the ¯). Using Equation 1, the GaAs "crystal hackle constant" was therefore estimated as $_{))}$=1.58 MPa√m; this parameter is analogous to the "mirror constant" used in isotropic materials. No obvious differences were observed between origins 'at the edge' vs. 'away from the edge', although the data appeared to be more consistent for cracks that originated away from the edge. The apparent absence of a correlation between origin location and fracture strength suggests that the sample edges are smooth with relatively few defects.

We therefore find that Orr's relation (Equation 1) can be generalized to single crystal GaAs, were the parameters are defined in reference to the crystallographic directions that dominate the fracture mechanism:

$$_{))110\}} \quad (4)$$

where σ_f is the fracture strength, $_{110\}}$ is the crystal hackle radius, and $_{))}$ is the crystal hackle constant.

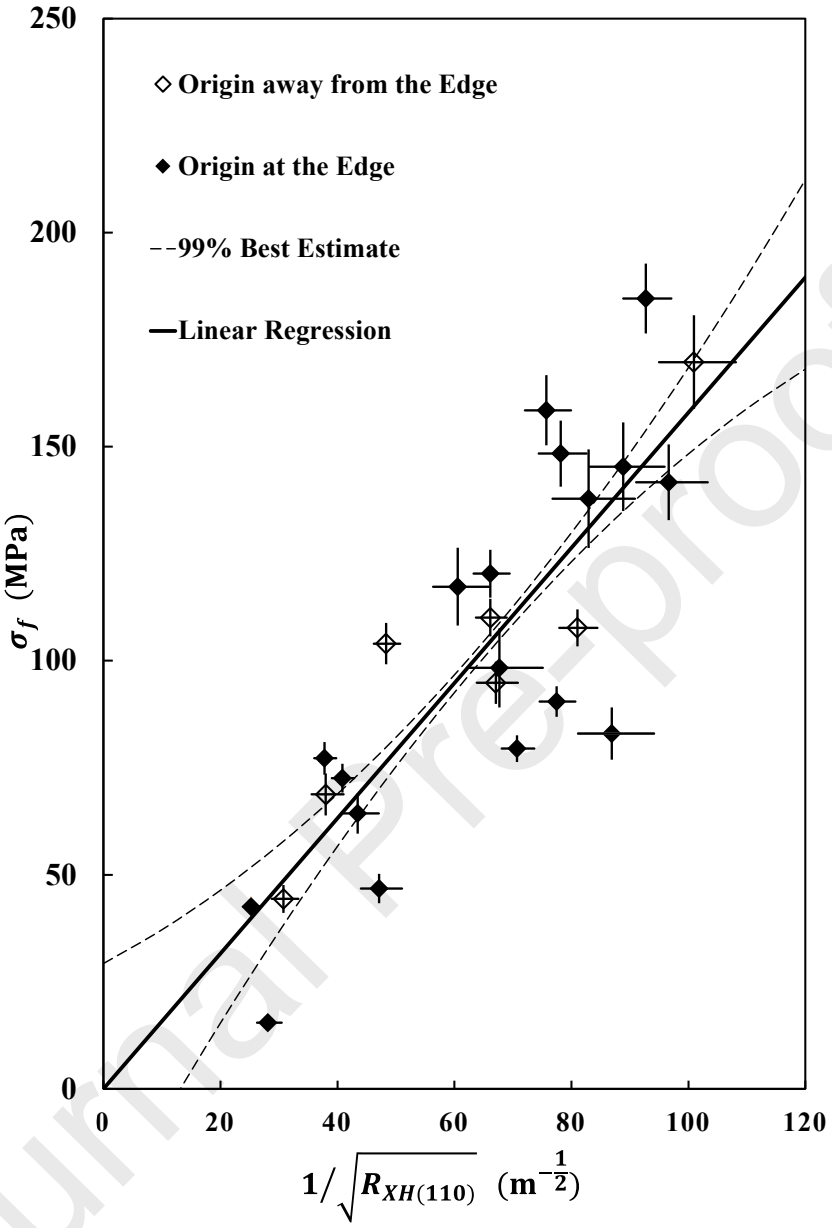

Figure 10: Relationship between fracture strength and the crystal hackle radius for the main (110) GaAs fracture mirror (data for all tested samples). R^2=0.71 for the linear regression.

Radial lengths associated with the 'mirror-branching' boundary correctly predicted the fracture strength within 19% from the measured values. From a practical perspective, where the lateral resolution of the instruments used to detect the mirror-hackle boundary was not sufficient, the hackle height could be measured at least at 2 different radial

locations and then used to extrapolate the hackle constant, as shown for a representative sample in Figure 11 .

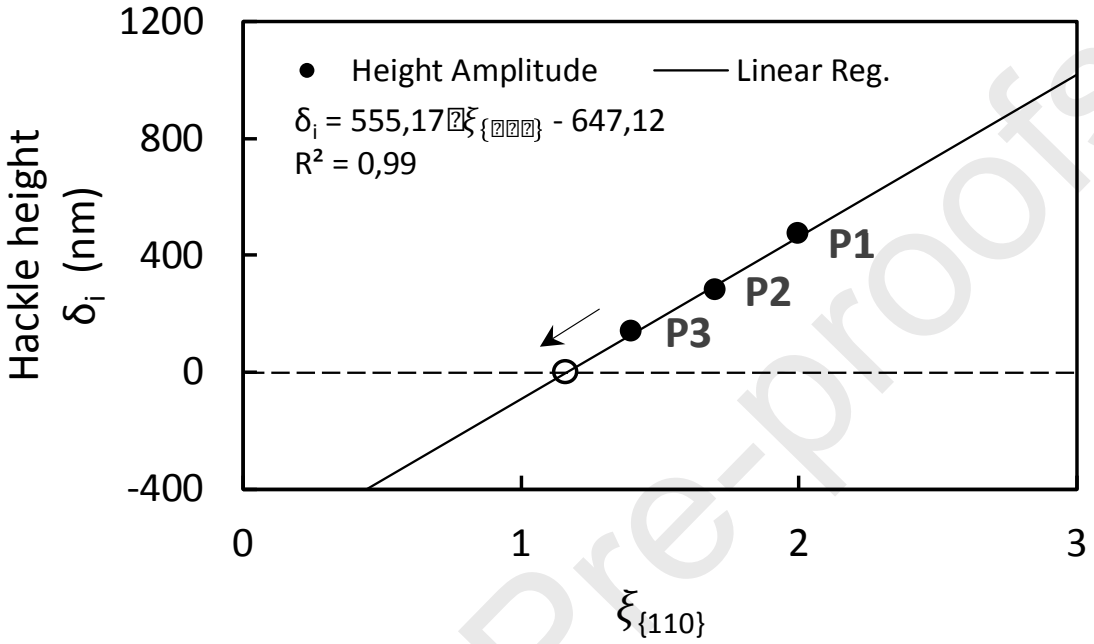

Figure 11: Relationship between hackle height featured at branching and normalized radial distance-to-crystal hackle radius ( ) for the main (110) GaAs fracture ($R_{XH\{110\}}$=151μm, σ_f=83±6MPa).

For the representative example in Figure 11, the normalized radial length, , and correspondent hackle's height available at P1, P2, and P3, were used to estimate the hackle radius ($R_{XH\{110\}}$=151μm) and a discrepancy of 16% was incurred between this method and the directly measured hackle radius.

IV. DISCUSSION

Experimental evidence shows that it is not necessary to distinguish between 'edge crack origins' and 'origins away from the edge' when generalizing Orr's relation to single crystal

GaAs. This occurs because we include crystallographic references when defining the crystal hackle radius R_{XH} and crystal hackle constant A_{XH} that are analogous to the mirror radius and mirror constant in isotropic media.

From the experimental quantitative analysis, two sets of fractographic features were consistently recognizable, since they formed on different planes following the methodology and recommendations outlined in this study. For instance, while the first quasi-static set of GaAs terraces was due to the misalignment, the GaAs wing-like features at branching were due to dynamic crack growth effects where radial distances at critical branching scaled with the strengths.

A. GaAs Step-like Terraces

For quasi-static loading in brittle materials, the fracture surface is usually created in a direction orthogonal to the maximum tensile stress. In fact, steps initiate at the crack origin, depending on the flaw orientation or the cleavage plane alignment with the loadings. GaAs {110} steps occur when the principal stress was not perfectly aligned with the cleavage plane or when there were any other misalignments with the initial flaw. In this study, the GaAs steps occurred along the (110) planes, consistent with it being the weakest plane as reported in the literature[12,34–39]. Figure 2-3 showed that the GaAs (110) steps fan out from the origin where the crack velocity is nearly zero, which indicates that their formation is not related to dynamic effects. A similar mechanism has been reported for silicon single crystal because of a small misalignment of the main cleavage plane[40]. Kermode et al.[41] reported on a complex 'multi-scale' phenomenon in silicon single-crystals whereby very low-speed crack propagation occurs on the (110) plane (i.e. after cracks decelerate). Cleavage steps are caused by the crack propagating on very close parallel planes and it is usually one or more single lines, parallel to the local direction of crack propagation[17]. They are running radially towards the surface in compression and are not materially affected by the crack-front dynamics. Although the fractographic features associated with misalignments were not used to estimate the samples' strength, they were helpful in locating the fracture origins.

B. Dynamic Crack Branching

Once the crack-tip reaches a critical speed, the crack-tip branches on more energetically favorable cleavage planes. The crack evolves according to the crystal anisotropy and the crack-tip speed, thereby minimizing the energy involved in the fracture process. GaAs hackle marks consistently form at a distance inversely proportional to the stress squared (see Eq. (1) and Figure 10) in the direction ¯. The fractography of GaAs surfaces suggested that combinations of small prisms-like features were created as an energy dissipation mechanism and were not due to random defects or misalignment, as they systematically mark the surface for a range of 2° with respect to the free surface.

As the crack-front becomes dynamically unstable, it branches away from the {110} planes toward particular families of planes, including {331}, {231}, {221}, {241}, {130}, {131}, {121}, {111}, {142}, {132}. Large hackles consolidate on those planes that minimize the system's energy during propagation, thus explaining why the {111} crack-tip deflection family of planes is shown to dominate for the GaAs single crystal (e.g. D1 shows mostly {111} in Figures 7-8). This observation is consistent with the understanding that the fracture toughness on the (111) plane, $K_{1c(111)}$ = 0.39 MPa√m, and on the (110) plane, $K_{1c(110)}$ = 0.46 MPa√m, have similar magnitudes[42,43]; a crack can therefore easily switch between the (110) and {111} planes upon obtaining enough kinetic energy[21,42,43].

Moreover, surface profilometry of the features formed after branching reveal that the hackle height approximately scales with the distance from the branching location. Assuming that the crack velocity does not change considerably after first branching for a given direction, then it could be inferred that the hackle height scales linearly with the crack's energy release rate (ERR). In this work, stereography and analytical geometry helped confirm that both φ_i and θ_B were consistent with the (001) stereograms found in literature[32]: both planes and axis zones followed the Weiss rule for a range of crack-branching radius directions (Figure 9). Features on planes other than (110) cannot be associated with misalignment or defects, since the fractographic features consistently start at a distance inversely proportional to the stress squared for nearly the same ¯ hackle radius directions with respect to the free surface (Fig. 10). These are in good agreement

with another reported surface instability previously reported in GaAs ("fork-shaped" sinking[44]) and analogous to "V-shape markings" in single crystal silicon[20,45].

V. CONCLUSION

This manuscript provides a systematic approach to estimate the strength of fractured GaAs single crystals by generalizing Orr's relation for isotropic media to single crystals. Standard fractographic methods typically employed in homogeneous, isotropic materials were adapted to study anisotropic, single-crystal GaAs fractured by uniaxial loading. "Terrace-like" step features were identified and explained as a quasi-static mechanism with which the crack-front re-aligns with the direction orthogonal to the maximum tensile stress (i.e. cleavage plane misaligned with loading). These step-like features were also used to locate the effective crack origin. A new characteristic parameter, the "crystal hackle radius" R_{XH} (analogous to the "mirror radius" in isotropic materials) was defined as the distance from the origin to the "mirror-branching" boundary which coincided with the macroscopic {111} deflection of the crack-front predominantly aligned with ¯. This framework extends Orr's empirical relation for isotropic media to GaAs single crystals and establishes the correspondent "crystal hackle constant" $_{))}$= 1.58 MPa√m to estimate the strength (analogous to the "mirror constant" in isotropic materials). It was noted that hackles form at distinct values of the energy release rate (ERR). Microscopic investigation reveals that the mirror-branching corresponds to specific, well-defined planes formed as the dynamically unstable crack-front deviates from the initial {110} plane. Hackle lines were found to be explained by combinations of well-defined crystallographic planes. The hackles initially correspond to many different planes but ultimately consolidate mostly along the {111} family of planes as the crack develops. The crystallographic families of planes along which crack growth was observed follows the Weiss zone law, as illustrated using stereographic projections.

FUNDING

The authors would like to thank the Natural Sciences and Engineering Research Council of Canada (NSERC) Discovery Grant RGPIN-2015-04185, MITACS Globalink Grant IT09006, and the ÉTS Fonds pour la collaboration international de recherche for funding.

REFERENCES

1. Blakemore, J. S. Gallium arsenide. *Key Pap. Phys. ; no. 1* **44**, 401 p. (1987).
2. Hjort, K., Soderkvist, J. & Schweitz, J. A. Gallium arsenide as a mechanical material. *J. Micromechanics Microengineering* **4**, 1–13 (1994).
3. Green, M. A., Emery, K., Hishikawa, Y., Warta, W. & Dunlop, E. D. Solar cell efficiency tables. *Prog. Photovoltaics Res. Appl.* **23**, 1–9 (2015).
4. Konagai, M., Sugimoto, M. & Takahashi, K. High-efficiency GaAs thin film solar cells by peeled film technology. *J. Cryst. Growth* **45**, 277–280 (1978).
5. Dushkina, N. M. Dicing of Gallium Arsenide (GaAs) Wafers with the Laser MicroJet ® Challenges , Improvements and Safety Issues. *Engineering* (2015).
6. Rice, R. W. Fracture Topography of Ceramics. in *Surfaces and Interfaces of Glass and Ceramics* 439–472 (Springer US, 1974). doi:10.1007/978-1-4684-3144-5_24
7. Zapffe, C. A. & Worden, C. O. Fractographic study of an ammonium dihydrogen phosphate single crystal. *Acta Crystallogr.* **2**, 383–385 (1949).
8. Zapffe, C. A. & Worden, C. O. Further fractographic studies of synthetic single crystals. *Acta Crystallogr.* **2**, 386–388 (1949).
9. Zapffe, C. A. & Worden, C. O. Fractography as a technique in crystal chemistry. *Acta Crystallogr.* **2**, 377–382 (1949).
10. Tsai, Y. L. & Mecholsky, J. Fracture mechanics description of fracture mirror formation in single crystals. *Int. J. Fract.* **57**, 167–182 (1992).
11. Shetty, D. K., Bansal, G. K., Rosenfield, A. R. & Duckworth, W. H. Criterion for Fracture-Mirror Boundary Formation in Ceramics. *J. Am. Ceram. Soc.* **63**, 106–108 (1980).
12. Margevicius, R. W. & Gumbsch, R. Influence of crack propagation direction on

(110) fracture toughness of gallium arsenide. *Philos. Mag. A Phys. Condens. Matter, Struct. Defects Mech. Prop.* **78**, 567–581 (1998).

13. Okui, T., Hasegawa, S., Fukutome, H. & Nakashima, H. Shearing orientation dependence of cleavage step structures on GaAs(110). *Surf. Sci.* **448**, 219–224 (2000).
14. Sauthoff, K. *et al.* Nonlinear dynamic instability in brittle fracture of GaAs. *Phys. Rev. B* **60**, 4789–4795 (1999).
15. Orr, L. Practical Analysis of Fractures in Glass Windows. *Mater. Res. Stand.* **12**, 21–23 (1972).
16. ASTM. Standard practice for fractography and characterization of fracture origins in advanced ceramics. *ASTM Int.* 1–51 (2010). doi:10.1520/C1322-05BR10.2
17. Quinn, G. D. *NIST Recommended Practice Guide: Fractography of Ceramics and Glasses*. *National Institute of Standards and Technology; NIST Recommended* **191**, (NIST SP - 960-16, 2016).
18. Quinn, G. D. Guidelines for measuring fracture mirrors. in *Ceramic Transactions* **199**, 163–187 (2007).
19. Dugnani, R. & Zednik, R. J. Flexural strength by fractography in modern brittle materials. *J. Am. Ceram. Soc.* **96**, 3908–3914 (2013).
20. Sherman, D. Fractography of Dynamic Crack Propagation in Silicon Crystal. *Key Eng. Mater.* **409**, 55–64 (2009).
21. Sherman, D., Markovitz, M. & Barkai, O. Dynamic instabilities in (111) silicon. *J. Mech. Phys. Solids* **56**, 376–387 (2008).
22. Stewart, R. L. & Bradt, R. C. Fracture of single crystal MgAl204. *J. Mater. Sci.* **15**, 67–72 (1980).
23. Moulins, A., Ma, L., Dugnani, R. & Zednik, R. J. Dynamic crack modeling and analytical stress field analysis in single-crystal silicon using quantitative fractography. *Theor. Appl. Fract. Mech.* **109**, 102693 (2020).
24. Mecholsky, J., Freiman, S. W. & Rice, R. W. Fractographic Analysis of Ceramics. in *Fractography in Failure Analysis* 363-363–17 (ASTM International, 1978). doi:10.1520/STP38101S
25. Griffith, A. A. The Phenomena of Rupture and Flow in Solids. *Philosophical*

Transactions of the Royal Society A: Mathematical, Physical and Engineering Sciences **221**, 163–198 (1921).

26. Mecholsky, J. J., Freiman, S. W. & Rice, R. W. Fracture surface analysis of ceramics. *J. Mater. Sci.* **11**, 1310–1319 (1976).
27. Tsai, Y. L. & Mecholsky, J. Fractal fracture of single crystal silicon. *J. Mater. Res.* **6**, 1248–1263 (1991).
28. Dugnani, R. & Verghese, P. Failure analysis of modern silicon dice. *Int. J. Appl. Ceram. Technol.* **11**, 783–792 (2014).
29. ASTM. Standard Test Method for Flexural Strength of Advanced Ceramics at Ambient Temperature. *ASTM Int.* 1–19 (2013). doi:10.1520/C1161-13
30. MATLAB version 9.6.0.1174912 (R2019a) Update 5. (2019).
31. Hammond, C. *The Basics of Crystallography and Diffraction*. **21**, (Oxford University Press, 2015).
32. Whittaker, E. J. W. Electron Diffraction in the Electron Microscope. in *Crystallography* (ed. Edington, J. W.) 217–224 (Macmillan Education UK, 1981). doi:10.1016/b978-0-08-023804-3.50022-5
33. Edington, J. W. Electron Diffraction in the Electron Microscope. in *Electron Diffraction in the Electron Microscope* 1–77 (Macmillan Education UK, 1975). doi:10.1007/978-1-349-02595-4_1
34. Wasmer, K. *et al.* Nanoindentation cracking in gallium arsenide: Part I. in situ SEM nanoindentation. *J. Mater. Res.* **28**, 2785–2798 (2013).
35. Pouvreau, C. *et al.* Nanoindentation cracking in gallium arsenide: Part II. TEM investigation. *J. Mater. Res.* **28**, 2799–2809 (2013).
36. Ning, X. J., Perezt, T. & Pirouz, P. Indentation-induced dislocations and microtwins in GaSb and GaAs. *Philos. Mag. A Phys. Condens. Matter, Struct. Defects Mech. Prop.* **72**, 837–859 (1995).
37. Levade, C. & Vanderschaeve, G. Rosette microstructure in indented (001) GaAs single crystals and the α/β asymmetry. *Phys. Status Solidi Appl. Res.* **171**, 83–88 (1999).
38. Hirsch, P. B., Pirouz, P., Roberts, S. G. & Warren, P. D. Indentation plasticity and polarity of hardness on (111) faces of GaAs. *Philos. Mag. B Phys. Condens. Matter; Stat. Mech. Electron. Opt. Magn. Prop.* **52**, 759–784 (1985).

39. Wang, S. & Pirouz, P. Mechanical properties of undoped GaAs. III: Indentation experiments. *Acta Mater.* **55**, 5526–5537 (2007).
40. Sherman, D. Hackle or textured mirror? Analysis of surface perturbation in single crystal silicon. *J. Mater. Sci.* **38**, 783–788 (2003).
41. Kermode, J. R. *et al.* Low-speed fracture instabilities in a brittle crystal. *Nature* **455**, 1224–1227 (2008).
42. Michot, G., George, A., Chabli-Brenac, A. & Molva, E. Fracture toughness of pure and In-doped GaAs. *Scr. Metall.* **22**, 1043–1048 (1988).
43. Yasutake, K. *et al.* Fracture of GaAs Wafers. *Jpn. J. Appl. Phys.* **27**, 2238–2246 (1988).
44. Xu, L. *et al.* Mechanical behavior of undoped n-type GaAs under the indentation of berkovich and flat-tip indenters. *Materials (Basel).* **12**, 1192 (2019).
45. Ben-Bashat Bergman, L. & Sherman, D. On dynamic surface instabilities of cracks in brittle crystals. *Int. J. Eng. Sci.* **136**, 78–91 (2019).